Characterization of a photon-counting intensified active pixel sensor (PC-IAPS): preliminary results

Uslenghi, Michela, Bonanno, Giovanni, Belluso, Massimiliano, Modica, Angelo, Bergamini, Paolo

Michela C. Uslenghi, Giovanni Bonanno, Massimiliano Belluso, Angelo Modica, Paolo Bergamini, "Characterization of a photon-counting intensified active pixel sensor (PC-IAPS): preliminary results," Proc. SPIE 4498, UV/EUV and Visible Space Instrumentation for Astronomy and Solar Physics, (10 December 2001); doi: 10.1117/12.450055

Event: International Symposium on Optical Science and Technology, 2001, San Diego, CA, United States

Characterization of a Photon Counting Intensified Active Pixel Sensor (PC-IAPS): Preliminary results

Michela Uslenghi[a], Giovanni Bonanno[b], Massimiliano Belluso[b],
Angelo Modica[c], Paolo Bergamini[d]

[a]Istituto di Fisica Cosmica "G.Occhialini"- CNR, Via Bassini 15, 20133 Milano, Italy
[b]Osservatorio Astrofisico di Catania, Via S. Sofia 78, 95123 Catania, Italy
[c]Xilinx Ireland, Logic Drive, Citywest Business Campus, Saggart, Dublin, Ireland
[d]Corning, Viale Sarca 222, 20126 Milano, Italy

ABSTRACT

We report about preliminary results of the characterization of a new kind of MCP-based detector: a Photon Counting Intensified Active Pixel Sensor (APS). PC-IAPS appears as the natural evolution of the Intensified CCD, maintaining the basic characteristics, but with improved performance in terms of dynamic range, along with some other appealing properties: higher radiation hardness, more compact design, lower requirements on the external electronics, low power consumption. The prototype we realized is currently in an early stage of development. Nevertheless, it allows us to demonstrate the feasibility of the photon counter and to measure some of the basic parameters. Some of the characteristics of the APS, relevant to the use in intensified systems, are analyzed and compared with the CCD ones, demonstrating the potentiality of the new device and allowing us to set the basis of future development.

Keywords: UV Detectors, Intensifiers, Intensified CMOS-APS, MCP detectors, Astronomy.

1. INTRODUCTION

MCP based detectors are the most commonly used Ultraviolet photon counting devices for astronomy[1,2,3,4,5], due to the high quantum efficiency (depending on the wavelength range even more than 50%), solar blindness, low background (< .1 counts/s·cm^2), large format (> 2000 x 2000 pixels), high resolution in space (< 15 μm) and time (down to ~0.1 ns). Several readout systems have been developed depending on the particular application, each one allowing to exploit one or several characteristics of the MCP intensifiers. Photon Counting Intensified CCDs[6,7](PC-ICCDs), in particular, which use a fast scan CCD as a readout system, exhibit the best spatial resolution (better than 3 μm), well higher than that allowed for the MCP currently available. Thus, the resolution of the PC-ICCDs is now limited by the intensifier, but the newly developed Silicon MCP[8] will likely offer, among a number of other advantages (lower background, wider choice of photocathodes, larger area, better uniformity), smaller pore diameter (down to 2 μm).

The main limitation of the PC-ICCD is the low local dynamic range, which is limited by the frame rate: in fact, photon events overlapping within a single CCD frame period are lost. CCDs generally used for this kind of application have frames rate that generally do not exceed 10-100 Hz, with format of about 512 x 512 pixels, or slightly less. Higher frame rate CCDs, developed for adaptive optic sensors, are available, but with a limited number of pixels (<128 x 128) and small formats, resulting in a reduced resolution and in a mismatch with the format of the MCP. In order to raise the frame rate, with the same number of pixels, we need a CCD with multiple outputs, since the frame rate is proportional to the number of ports (unfortunately, the amount of external circuitry increases accordingly), or a new kind of device with an a new kind of readout architecture.

The CMOS Active Pixel Sensor is a relatively new technology, not yet exploited in scientific applications due to the low image quality of the images. However, for this particular application we do not need high cosmetic characteristics, instead the high readout speed resulting from the intrinsically parallel architecture, together with the reduced electronics required to control the device (APS can be driven by digital circuitry and the A/D converter can be integrated on the

UV/EUV and Visible Space Instrumentation for Astronomy and Solar Physics, Oswald H. W. Siegmund, Silvano Fineschi, Mark A. Gummin, Editors, Proceedings of SPIE Vol. 4498 (2001)

chip, in which case both the input and the output signals are digital), could allow us a substantial improvement on the similar Intensified CCDs with a less complex electronics.

2. DETECTOR OVERVIEW

The detector architecture (figure 1) is basically similar to that of a Photon Counting ICCD. A Z-stack MCP intensifier, operating in the saturated regime, produces a spot of several millions of optical photons on a phosphor screen for every photon detected. Then a CMOS APS, optically coupled to the phosphor screen, records the image. A dedicated digital processing unit analyzes each frame, searches for valid events and computes the relative coordinates.

We used the setup of a PC-ICCD developed *at Istituto di Fisica Cosmica "G.Occhialini"* in collaboration with the *Dipartimento di Ingegneria Elettronica e Informatica* of the *Padua University* and described in Ref. [9,10,11], changing the readout system to an APS. This results in the fact that the two basic parts of the detector, the intensifier head and the readout system, are not well matched, because the intensifier is optimized for the CCD camera. However, even if the conditions are not optimal, we were interested in a first evaluation of the possibility of this system in order to better plan the subsequent development.

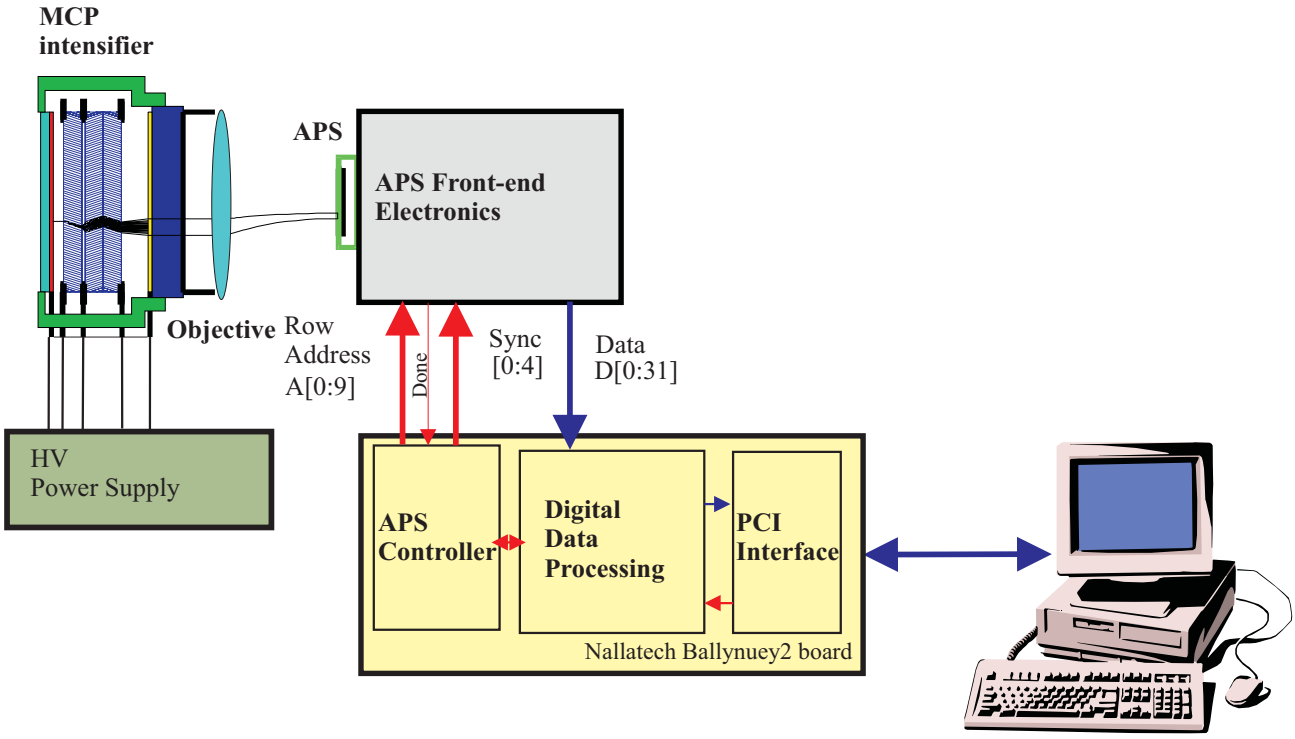

Figure 1. Block Diagram of the PC-IAPS.

The image intensifier used is a sealed Z-stack intensifier produced by Photek (MCP340), based on 40 mm diameter plates with 10 μm pores at 12 μm pitch. A P20 phosphor screen is deposited on a fiber optic (FO) faceplate. A RbTe photocathode, deposited on a MgF_2 input window allows to improve the quantum efficiency in the classical ultraviolet. The electron cascade generated by the MCP stack is transduced, via a phosphor screen and a relay optics system (an HR-Heligaron 35 objective manufactured by Rodenstock, with a numerical aperture of 0.32) with 1:4.3 demagnification ratio onto the APS array, a Photobit PB-1024, with 10 μm square pixel (6×9 μm^2 active area[12]) and 1024×1024 pixels format. This sensor, due to the 1024 8 bit A/D converters integrated on the chip and the eight parallel digital output ports, is able to provide up to 500 frames/s full frame and allows windowing with random access of the rows[13].

The APS is mounted on a prototyping board which provides the biases and the buffers for the signals from and to the device. Multiplexers are also present in order to pack the 64 output bits in 32 bit words. A commercial PCI board

(Nallatech Ballynuey2), provided with a XILINX FPGA (Virtex XCV300) user-programmable by downloading the configuration file from the PCI bus, is used to acquire and analyse the APS data output in real time.

The FPGA based digital data processing system acquires the eight digitised outputs of the APS as to generate, through a proper system of delays, 3×3 pixel windows that sweep dynamically the whole APS matrix at the pace of the pixel clock. The processing system performs in parallel the following tasks on each window:

i) check, according to appropriate discrimination and pile-up rejection criteria, for the presence of a charge distribution representing a photon event. At the moment, only a lower and an upper threshold are used as event criteria;

ii) compute the centroid coordinates with a resolution of 1/32 of a pixel, applying a simple centre of gravity algorithm to the charge distribution in the current window. The centroid coordinates of the charge distribution identified as a photon event are subsequently transferred to the memory of the PC.

Two detector operating modes have been implemented:

a) a 'frame grabber mode', where the frames, as they are generated from the APS, are simply transferred to the memory of the host PC;

b) a 'centroiding mode', where the collected photons are recorded in real-time as a list of event coordinates in series with tags marking the end of each frame; off-line data processing allows to compute the actual photon time tags from the frame number associated with each event, providing the time coordinate.

Some routines for data acquisition have been written in C, whereas the programs for the data analysis have been developed in Interactive Data Language (IDL).

A more detailed description of the PC-IAPS is given in an other paper in these proceedings[14].

3. PHOTON EVENTS

The gain of the intensifier is not well matched to the APS range (the design of the intensifier was optimized for the ICCD). Moreover, the APS itself shows a high noise level with a high fixed pattern component, dependent on the illumination level, which could indicate that the readout electronics needs further optimization, and a clear even/odd effect (even pixel values are more probable than the odd ones). The resulting signal-to-noise ratio is quite low and even if it is sufficient for the event detection and recognition, it strongly affects the accuracy of the centroid computation, preventing us from reaching sub-pixel accuracy.

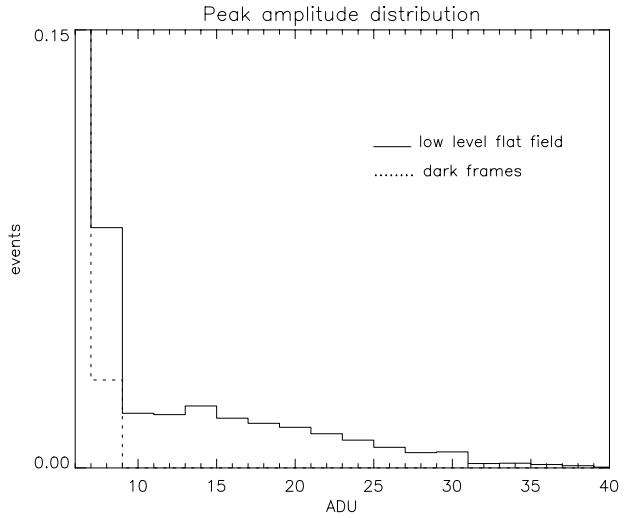

Figure 2. Peak value distribution of the photon events. For comparison, the pixel value distribution in dark frames is also given (dotted line).

In Fig.2 the distribution of the peak amplitude (binned to 2 ADU to eliminate the even/odd effect) is reported, for a CMOS clock frequency of 2.5 MHz (corresponding to 19 frames/s). For comparison, the distribution of the pixel values in a dark frame is also reported: there are not any pixel with value grater than 8 ADU. However, when the device is under a higher illumination level, the noise rises and the noise distribution shows a longer tail that is not easy to discriminate from the photon event distribution. In order to be conservative we set the lower threshold to 15 ADU. We also tried to use the device at higher frequency (7 MHz, corresponding to 50 frames/s): under these conditions the noise is slightly larger, therefore we set the threshold to 20 ADU. The upper threshold is set to 96 ADU.

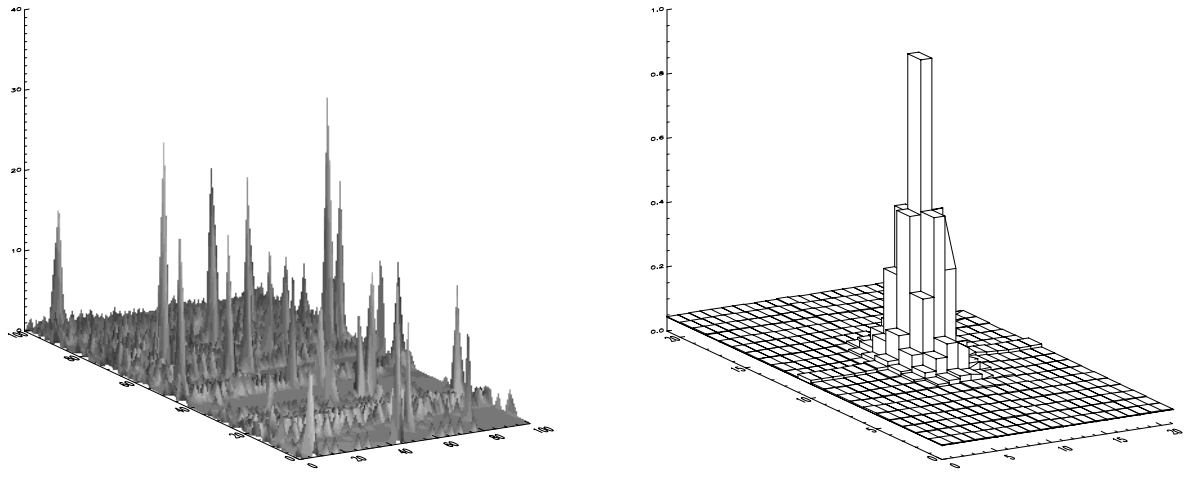

(a) **(b)**

Figure 3. (a) - Section of a frame where several photon events can be distinguished above the noise (a pattern noise is clearly apparent along one of the axes); **(b)** - Mean event shape, obtained by co-adding about 4,000 windows (21x21 pixels) centered on event peaks.

In Fig.3(a) a section of a frame is shown in a 3D view. The peaks produced by the photon events are clearly visible and are easily distinguishable from the background. The pattern noise is also clearly apparent as rows with pixel values systematically higher than the mean value of the background.
In Fig.3(b) the shape of the 'mean event' is reported. It has been obtained by summing about 4,000 windows of 21x21 pixels, each one centered on an event peak. The shape is approximately gaussian and is the result of the convolution of three terms:

- the distribution of the optical photons emitted by the phosphor screen at the output of the image intensifier
- the PSF of the optical system used to image the phosphor screen onto the APS array
- the response of the APS pixel.

The second term is not negligible. In fact, the size of the event clouds was previously measured coupling a CCD camera directly onto the output fiber optic window[9] (ratio 1:1). We could verify that the average photon event footprint is roughly oval. The mean σ dimensions are 19.8 ± 2.5 μm and 15.3 ± 0.4 μm along major and minor axis. With the 4.3 demagnification ratio introduced by the Rodenstock objective, we need to slightly defocus the events in order to sample the bright spots with the 10 μm APS pixel.

Regarding the last term, differently from the CCD pixel, for which we can assume a fill factor of 1, the sensitive area of an APS pixel is significantly limited by the preamplifier circuitry: in general is about 20-60% of the total pixel area and often has a complex shape, principally an L-shape. This fact produces some consequences on the precision of the centroid algorithms, as explained in section x. In the case of the photobit PB-1024 the sensitive area is a rectangle of 9 (in the x direction) × 6 (in the y direction) μm^2. Then, if the distribution of the optical photons emitted by the phosphor

screen and imaged on to the APS array can be assumed as a bi-dimensional gaussian, not necessary symmetrical, the signal detected from each APS pixel is the bi-dimensional gaussian integrated over the sensitive area.

In order to estimate the main parameters of the events, we illuminated the detectors with a low level flat field. Then a large number of events (about 10,000), extracted from several frames, were fitted with the function:

$$f(x,y) = g(x,y) \otimes P(x,y) \tag{1}$$

where:

$$g(x,y) = \frac{A}{2 \cdot \pi \cdot \sigma_x \cdot \sigma_y} \cdot e^{-\frac{(x-x_0)^2}{2 \cdot \sigma_x^2}} \cdot e^{-\frac{(y-y_0)^2}{2 \cdot \sigma_y^2}} \tag{2}$$

is the bi-dimensional gaussian and:

$$P(x,y) = \begin{cases} 1 & x, y \in S \\ 0 & x, y \notin S \end{cases} \tag{3}$$

is a first order model of the pixel response (S is the active area). Figure 4 shows the distributions of the event σ in the x and y direction: note that the shape of the spot on the APS array is symmetric, 0.8±0.16 pixel in x and 0.82±0.16 pixel in y.

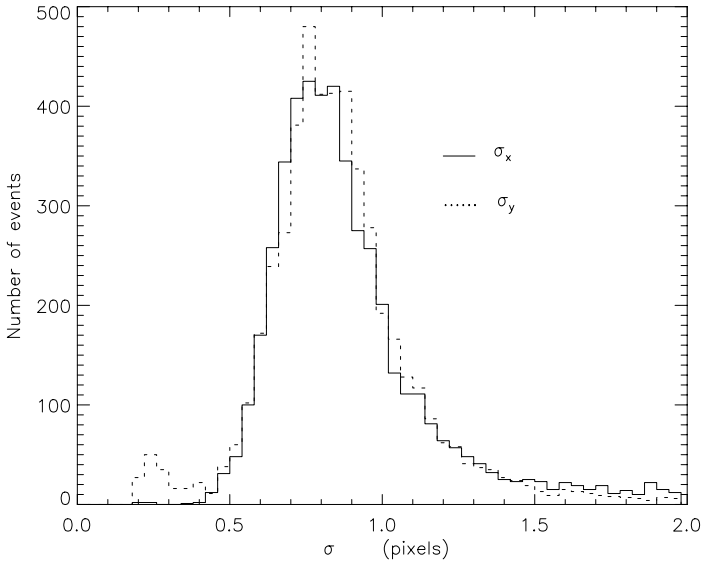

Figure 4. Event size distribution in the x and y directions, as derived by the gaussian fit.

4. CENTROIDING ALGORITHM

The centroid finding computation is affected by both systematic and stochastic errors. The latter are due to the noise and obviously depend on the signal-to-noise ratio. On the other hand, the choice to limit the sampling of photon event footprint to a few pixels (under-sampling) and to employ a truncated weighting algorithm (windowing) is known to introduce systematic shifts of the computed event coordinates with respect to the true ones. Whereas the errors introduced by the noise cannot be eliminated and degrade the spatial resolution, the systematic shift can be greatly

reduced, for example using the empirical techniques described in Ref. [7,15]. In effect, the two kind of errors are not independent, as we discuss in the following, and big systematic deviation can result in a larger noise-induced error.

The problem of the systematic errors affecting the algorithms used for event centroiding has been treated by several authors[7,16,17]. We show here the effect of the reduced fill factor of the APS pixels with the currently adopted algorithm, the classical 3-point center of gravity formula:

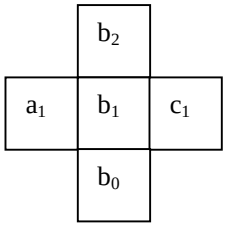

$$x_c = \frac{c_1 - a_1}{a_1 + b_1 + c_1} \qquad y_c = \frac{b_2 - b_0}{b_0 + b_1 + b_2} \tag{4}$$

In first approximation, we can consider the x and y computation separately, and reduce the problem to the uni-dimensional case. Both the under-sampling and the windowing effects are strongly dependent on the width of the event and on the position of the center inside the pixel. Figure 5 shows the combined effect of these two errors versus the σ of the events, expressed in pixels, for events centered in a fixed position (0.25 pixel, with the origin of the coordinates at the center of the pixel). The solid black line represents the systematic error for the CCD pixel (assuming a fill factor=1), the dotted blue line and the dashed green line represent the APS PB-1024 case, respectively in the x and y direction.
The behavior is similar in the three cases: at low σ the under-sampling error is dominant and decreases as σ increases. Then, after reaching a minimum, the window effect becomes prevalent and the systematic error increases monotonically with the event width. As we can expect, the fill factor plays a role mainly in the under-sampling regime, where the error associated to the y computation is significantly higher than the one associated to the x coordinate, which in turn is higher than for the CCD case (for example, for σ=0.3 and x=0.25, the systematic errors are, respectively: 0.14, 0.08 and 0.05 pixel). The windowing error, on the other hand, is not much affected by the fill factor. Thus, the optimum event width occurs at slightly larger σ for a lower fill factor.

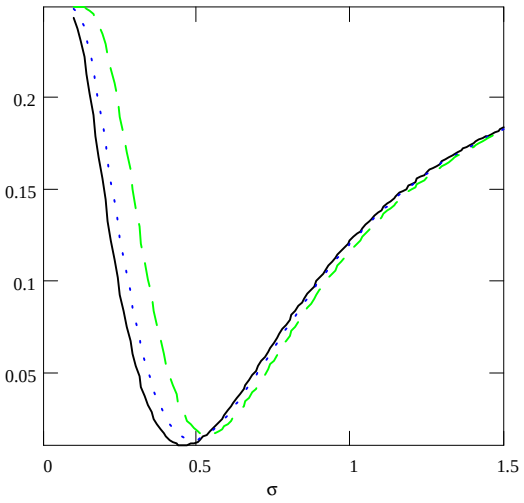

Figure 5. Centroiding systematic errors (expressed as fraction of pixel) versus event width for events centered at x=0.25 pixel (the origin of the coordinates is at the center of the pixel containing the peak), for three different fill factors: 1, or CCD pixel (black solid line); 0.9, or APS in x direction (blue dotted line); 0.6, or APS in y direction (green dashed line).

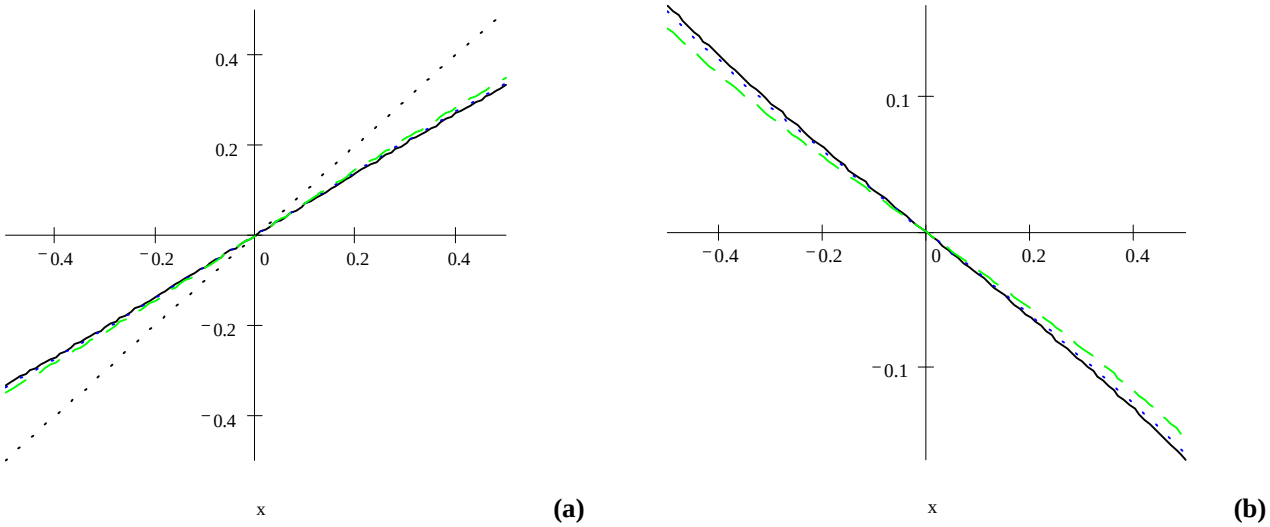

Figure 6. **(a)** – Response of the algorithm for σ=0.8 pixel events (the dotted black line represents the linear response) versus the event position along the pixel; **(b)** – Related errors. Solid black line: CCD; blue dotted line: APS-x; green dashed line: APS-y. The units are fractions of pixel.

In our case, with σ~0.8 pixel, the events are larger than the optimum and the windowing is not negligible. Figure 6(a) shows the response of the algorithm, for σ=0.8 pixel, varying the position of the 'true' event center along the pixel (in the three cases: CCD pixel, APS x and APS y); the plot in Fig.6(b) represents the associated error.

The effect of the noise is more complex and requires a good knowledge of the noise as well as taking in account the distributions of the characteristic parameters of the events (amplitude, shape and size).

However, we can get some ideas about the phenomenon by applying the error propagation to the centroid formula applied on a 'mean' event (amplitude integrated on both directions=120 ADU, that correspond to a peak value close to our threshold for σ=0.8 pixel in both directions), assuming a simple model of noise, a poissonian distribution with standard deviation 3 ADU (corresponding to the value we measure clocking the APS at 2.5 MHz) and a 3.4% of pixel non-uniformity. Moreover, the (imperfect) digitization of the data has been taken in account. The plot in Fig.7(a) shows the result of the error propagation for σ=0.8 pixel. This is the error associated to the computed coordinate, which is related to the error on the 'true' coordinate (presented in Fig.7(b)) by:

$$\sigma_{x_{true}} = \sigma_{x_c} \cdot \left(\frac{dx_c}{dx_{true}} \right)^{-1} \tag{5}$$

From this relation we can see the importance to reduce the systematic deviations of the algorithm response from the linearity to the minimum. In fact, the second term is 1 only in the ideal case, when $x_c=x_{true}$; both windowing and undersampling contribute to increase its value. Fig.7(c)-(d) and Fig.7(e)-(f) show the same plots for two different cases: an event with optimum width and an event with σ=0.3 pixel (undersampling dominated) respectively, all the other parameters being unchanged.

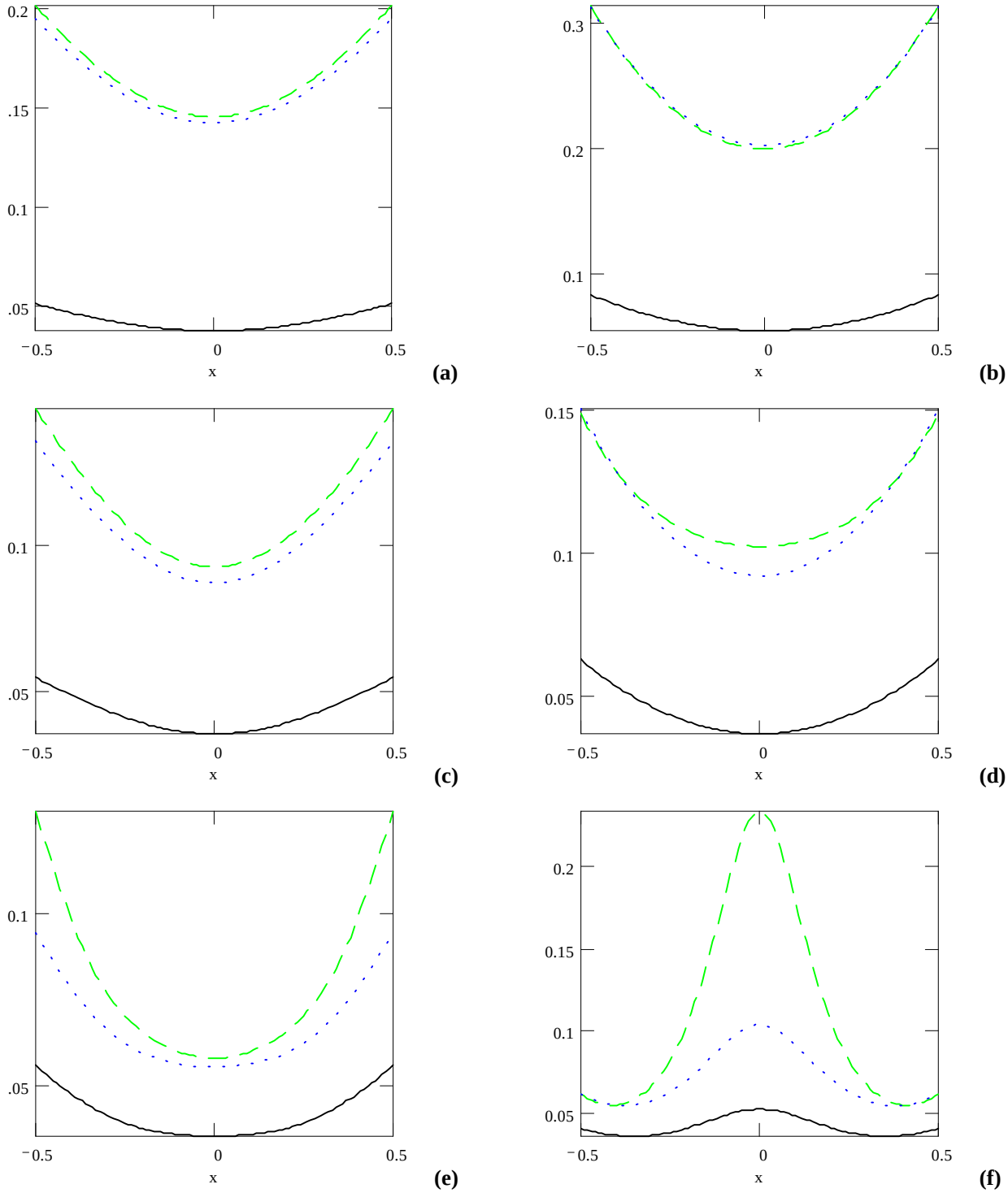

Figure 7. Left panels: error associated to the calculated coordinates as a function of the event position, for σ=0.8 pixel **(a)**, σ=0.5 pixel **(c)**, σ=0.3 pixel **(e)**; Right panels: error associated to the 'true' coordinates as a function of the event position, for σ=0.8 pixel **(b)**, σ=0.5 pixel **(d)**, σ=0.3 pixel **(f)**. Solid black line: CCD; blue dotted line: APS-x; green dashed line: APS-y. The axes units are in pixels.

The errors reported in these plots are a considerable fraction of the physical pixels: that seems to prevent us from sub-pixel centroiding to restore the MCP resolution. In effect, this is due to the low signal-to-noise ratio, and in particular, to the low intensifier gain. Assuming a σ=0.5 pixel, but with an integrated event amplitude=450 ADU (corresponding to a peak value of 128 ADU for the event with coordinates in the middle of the pixel, that is a good matching between intensifier and readout sensor), the error is less than 1/25 pixel in both directions (Fig.8).

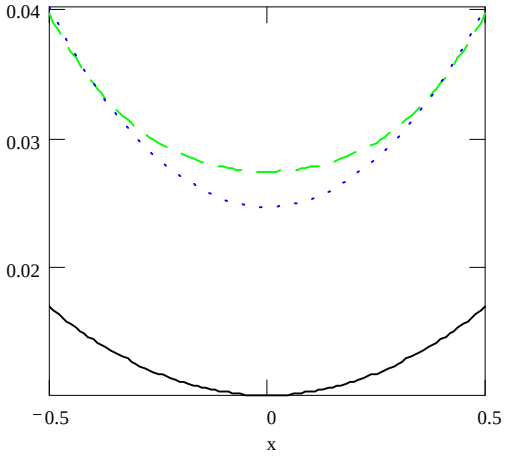

Figure 8. Error associated to the centroid coordinates as a function of the event position, for events of optimal size and amplitude. Solid black line: CCD; blue dotted line: APS-x; green dashed line: APS-y. The axes units are in pixels.

5. SPATIAL RESOLUTION

To check the imaging property of the detectors we projected a spot onto the photocathode (Fig.9). A lower limit for the spatial resolution can be set by the FWHM of the projected spot (58 μm). The image of the pinholes, in fact,is the result of the convolution of three terms:

a. the PSF of the optical system in front of the detector
b. the PSF of the proximity focus of photocathode
c. the PSF of the readout system

We can assume that the first one is negligible. The two last terms, combined, define the PSF of the detector.

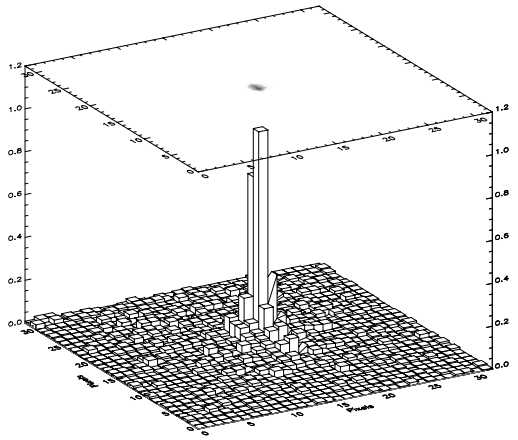

Figure 9. Projected pin-hole.

A standard USAF test target has also been projected, and a section is shown in Fig.10.

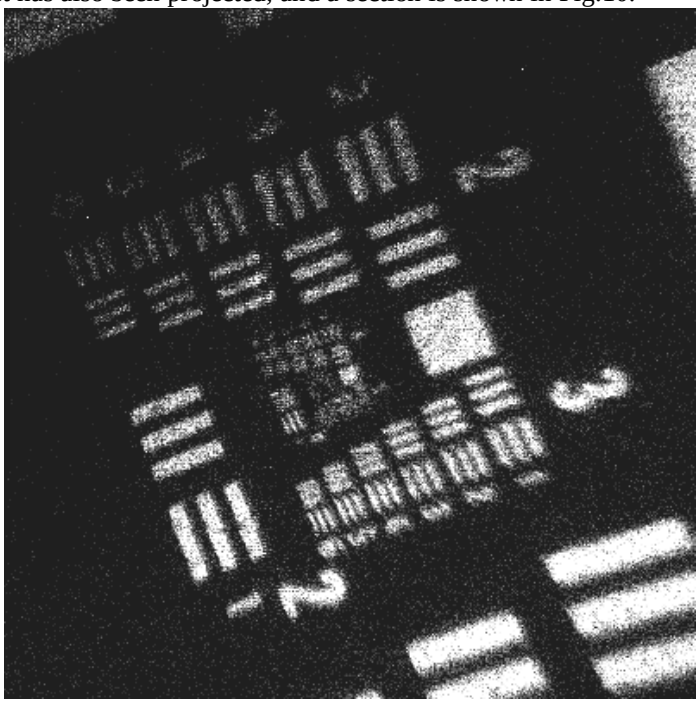

Figure 10. Projection of a standard USAF test target projected onto the detector.

6. DYNAMIC RANGE

The dynamic range properties of MCP-based photon counting detectors are usually described in terms of local and global dynamic, i.e. in terms of response to a point-like and to a diffuse uniform illumination, respectively. Microchannel plates are known to exhibit saturation effects due to the finite recharge time of MCP channels. These effects are strongly dependent on the extension of the illuminated area. The readout systems also exhibit some kind of limitation to the dynamics. Generally, the local and global dynamic response are limited, respectively, by the MCP gain saturation and by the readout processing electronics. For small spots imaging conventional MCPs, composed of channels with resistance > 10^{14} Ω, begin to suffer from gain sag at input count rate of less than 10-20 counts/channel/s, producing charge pulses below the detection threshold. The Z-stack MCP intensifier used in this prototype has been independently characterized with standard pulse processing electronics connected to the phosphor screen anode (as reported in Ref. 10), in response to point-like sources ranging from 40 to 700 μm in size (the DQE 10% loss occurs at count rate ranging from 690 and 18,900 counts/s), thus the behavior of the intensifier by itself is well known and the contribution of the readout system can be easily separated.

6.1 Local Dynamic Range

For the PC-ICCDs, the MCP intensifier sets the ultimate limit, but, in fact, the real limit is the readout time of a CCD frame, in order to avoid the confusion of multiple events at the same location. Overlapping events can be detected as single events or rejected, depending on the recognition algorithm implemented. In the first case, they generate spurious centroid positions, reducing the resolution, but improving the dynamic properties.

From the Poisson statistics it follows that, for a point-like source, the 10% fractional count rate loss occurs at about 1/10 of the frame rate. In fact, the ratio between detected events and total input counts is given by:

$$f(\mu) = e^{-\mu} \tag{6}$$

where μ is the mean number of events per frame. For typical CCD frame rate of 10-50 Hz, the 10% fractional count rate loss occurs for 1-5 counts/s sources. However, the algorithm presently adopted for the PC-IAPS prototype records multiple events as single. Therefore the ratio is:

$$f(\mu) = \frac{1}{\mu} \cdot \sum_{n} \frac{\mu^n \cdot e^{-\mu}}{n!} \tag{7}$$

and the 10% fractional count rate loss occurs at about twice the count rate. In effect not all the multiple events are recorded: if the number of overlapping events is too high, their sum exceed the upper threshold and is discarded, but this happens for n>5-6, for which the terms of the summation are negligible.

The results of the measurements of the dynamic response to a point-like source (projected size of 58 μm FWHM) are given in Fig. 11(a) for two different readout frequencies (2.5 and 7 MHz, respectively 19 and 50 frames/s). The 10% fractional count rate loss occurs at 5.75 and 16 counts/s (Table 1). Taking into account the number of channels illuminated these figures translate into a 0.3 and 0.8 count/s/channel, well below the limit set by the MCP intensifier alone. In fact, these value are in agreement with each other by scaling for the different frequencies (confirming that the dynamic is limited by the APS) and are about 50% higher than expected from the Poisson statistics. This discrepancy can be explained by the high lower threshold we set in order to reject the noise: it causes a non-negligible percentage of single events to be lost, but they are detected at the high count rate, when the overlap of multiple events push them above the threshold. For comparison, the results of similar tests carried out on the photon counting ICCD using the same MCP intensifier[10] are given in Table 1 (in this case, due to the good separation between the signal amplitudes and the noise distribution, and then the lower threshold, the agreement with the Poisson statistics is better).

6.2 Global Dynamic Range

For extended sources readout systems based on image sensors perform quite well compared to other devices, since they are not limited by the loss of simultaneous events which occur in different places on the MCP. PC-ICCDs can reach count rates higher than ~10^5 cts·cm^{-2}s^{-1}.

The tests of global dynamic range have been carried out using the flat field produced by a pin-hole (200 μm diameter) located 1.3 m from the detector. The field of view of the detector has been reduced from 4 to 2 cm in order to minimize the problem of the fixed pattern noise of the APS arising when the entire sensor is illuminated. Under these conditions, the 10% fractional count rate loss (see Fig.11(b) and Table 1) occurs at 13,000 counts/cm^{2}s (19 frames/s) and 33,000 counts/cm^{2}s (50 frames/s).

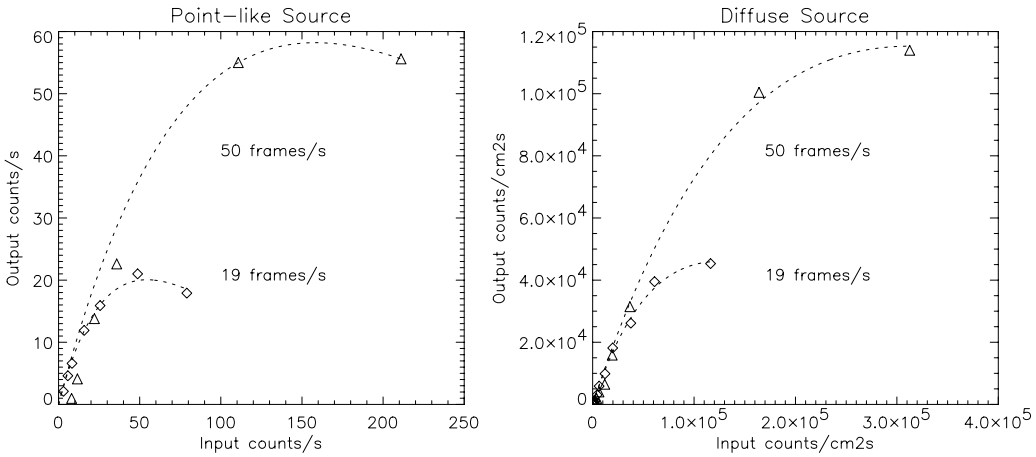

(a) **(b)**

Figure 11. Point-like source **(a)** and diffuse illumination **(b)** dynamic range.

	PC-IAPS		**PC-ICCD**[Ref.10]	
10% Fractional rate loss	19 frames/s (2.5 MHz)	50 frames/s (70 frames/s)	60 frames/s	220 frames/s
Point-like source (counts/s)	5.75	16	13	54
Diffuse source (counts/cm^{2}s)	13,000	33,000	26,000	92,000

Table 1. Dynamic performance summary. The characteristics of a PC-ICCD have also given for comparison.

7. CONCLUSIONS

We showed that the CMOS APS is a good candidate as a readout system for MCP-based detectors, allowing to maintain the best characteristics of the Intensified CCD, but with higher local dynamic range, time resolution, and radiation hardness, reduced complexity of the electronics and lower power consumption.

The prototype is in an early stage and needs some substantial improvements. We started the development of a new version of the electronics in order to run the APS at higher frequencies, keeping a reasonable noise level . Moreover, we will acquire a new intensifier, specially designed to match the characteristics of the APS. With these improvement we think we will be able to reach the spatial resolution intrinsic to the intensifier, as we showed in section 4, and to exploit the high speed characteristics of the sensor. The possibility to run the device at very high frequency is one of the most appealing features: an APS running at 500 frames/s, as the characteristics of the APS we adopted allows, can sustain a flux of 100 counts/s (or 200 counts/s with optimization of the event identification) with a loss of only 10%.

8. ACKNOWLEDGEMENTS

We would like to thank Mauro Fiorini for his support during the measurements and Armin Karcher for a critical reading of this manuscript.

REFERENCES

1. O. H. W. Siegmund, M. Lampton, J. Bixler, S. Chakrabarti, J. Vallerga, S. Boyer, R. F. Malina,, *J. Opt. Soc. Am. A* **3**, p. 2139, 1986
2. M. Clampin and F. Paresce, *Astron. Astrophys.* **225**, p. 578, (1989)
3. O. H. W. Siegmund, M. Gummin, J. Stock, G. Naletto, G. Gaines, R. Raffanti, J. Hull, R. Abiad, T. Rodriguez-Bell, T. Magoncelli, P. Jelinsky, W. Donakowski, K. Kromer, *Proc. SPIE* **3114**, p. 283, (1997)
4. R. A. Kimble et al., *Astrophys. J.* **492**, L83, (1998)
5. J.L.A. Fordham, D.A. Bone, M.K.Oldfield, J.G.Bellis,T.J.Norton, *Proc.ESA* **SP-356**, p.103, (1992)
6. P. D. Read, I. G. van Breda, T. J. Norton, R. W. Airey, B. L. Morgan, J. R. Powell, *Instrumentation for Ground-Based Optical Astronomy, Present and Future*, ed. L. B. Robinson, Springer-Verlag N.Y.,p. 528, (1988)
7. M. K. Carter, B. E. Patchett, P. D. Read, N. Waltham, and I. G. van Breda, *NIM* **A310**, p. 305, (1991)
8. O.H. W. Siegmund, A.S. Tremsin, J.Vallerga, C.P.Beetz, R.W. Boerstler and D.Winn, *Proc. SPIE* **4497**
9. P.Bergamini, G.Bonelli, S.D'Angelo, S.Latorre, L.Poletto, G.Sechi E.G.Tanzi, G.Tondello**,** M.Uslenghi Proc. SPIE, **3114**, 250, (1997)
10. P.Bergamini, G.Bonelli, E.G.Tanzi, M.Uslenghi, L.Poletto, G.Tondello, *Review of Scientific Instruments*, **71**, n.4, 1841, (2000)
11. P.Bergamini, G.Bonelli, A.Paizis, L.Tommasi, M.Uslenghi, G.Tondello, R.Falomo, *Experimental Astronomy*, **10**, n.4, 457, (2000)
12. C.Williams, Photobit, private communication
13. Photobit Corporation, PB-1024 Product Specification, August 1999.
14. G.Bonanno, M.Belluso, A.Calì, C.Timpanaro, M.Uslenghi, M.Fiorini, A.Modica, these proceedings *SPIE*, **4498**
15. J. G. Bellis, D. A. Bone and J. L. A. Fordham, *Pub. A.S.P.* **103**, p. 253, (1991)
16. A. Boksenberg, C. I. Coleman, J. L. A. Fordham, K. Shortridge, *Adv. Electronics & Electron Physics* **64A**, p. 33, (1985)
17. J. Dick, C. Jenkins, and J. Ziabicki, *Pub. A.S.P.* **101**, p. 684, (1989)